Boric Acid Nanotubes, Nanotips, Nanorods, Microtubes, and Microtips

Yan Li,[†] Rodney S. Ruoff,*[,‡] and Robert P. H. Chang*[,†]

Department of Materials Science and Engineering, Northwestern University, 2220 Campus Drive, Evanston, Illinois 60208-3108, and Department of Mechanical Engineering, Northwestern University, 2145 Sheridan Road, Evanston, Illinois 60208-3111

Received February 24, 2003. Revised Manuscript Received June 16, 2003

Thin films containing boron, carbon, and oxygen were synthesized by plasma-enhanced chemical vapor deposition (PE-CVD). When the thin films were exposed to humid atmosphere, nano- or micro-scale boric acid structures were observed to grow spontaneously. Depending on the relative humidity, temperature, and exposure time to the humid atmosphere, these boric acid structures were either nanotubes, nanotips, nanorods, microtubes, or microtips. X-ray photoelectron spectroscopy (XPS) studies on the thin film surface suggested that the thin films contained B_2O_3, BCO_2, and C−C clusters. The relative amounts of boron, carbon, and oxygen in the thin films were about 41.3, 14, and 43.9% respectively. Secondary ion mass spectrometry (SIMS) results indicated that the elemental distribution of boron, carbon, and oxygen in the thin films was rather homogeneous. X-ray diffraction (XRD) was used to study the time evolution of these boric acid structures at 23 °C and 45 ± 3% relative humidity. Scanning electron microscopy (SEM) and transmission electron microscopy (TEM) images of the structures showed that the boric acid tubes and tips had a hollow structure, whereas the boric acid rods were solid. The boric acid structures dehydrated into similarly shaped amorphous structures in a vacuum. In-situ X-ray diffraction studies in a vacuum showed that at 23 °C and 45 ± 3% relative humidity (at one atmosphere pressure), the dissociation rate law of the boric acid structures at 250 and 500 mTorr was $[-\ln(1-\alpha)]^{1/2} = kt$; whereas at 1000 mTorr, the dissociation rate law was $[-\ln(1-\alpha)] = kt$, where α, k, and t were the fraction of decomposed reactant, the reaction rate constant, and the time, respectively.

Introduction

Materials at the nano- and micro-scale lengths have unique structural, mechanical, electronic, and optical properties. They can be building blocks for various nano and micro devices. Nanotubes and microtubes can be used to store or transport substances. Several kinds of nano/micro tubes have been synthesized, such as BN[1] and carbon nanotubes,[2] and SiO_2,[3] MoS_2,[4] V_2O_5,[5] and ZnO[6] microtubes.

Orthoboric acid (H_3BO_3) is a layered material with a triclinic crystal structure,[7] as shown in Figure 1. Orthoboric acid is the most common form of boric acid, and the term "boric acid" will be used throughout this paper to mean orthoboric acid.[7] In each layer of the material, one boron atom is surrounded by three oxygen atoms to form triangular BO_3 groups, and hydrogen bonds link the planar BO_3 groups together. The layers are 0.318 nm apart and are held together by weak van der Waals forces. The unique structure of boric acid is similar to those of graphite and MoS_2, and boric acid is also capable of acting as a lubricant.[7]

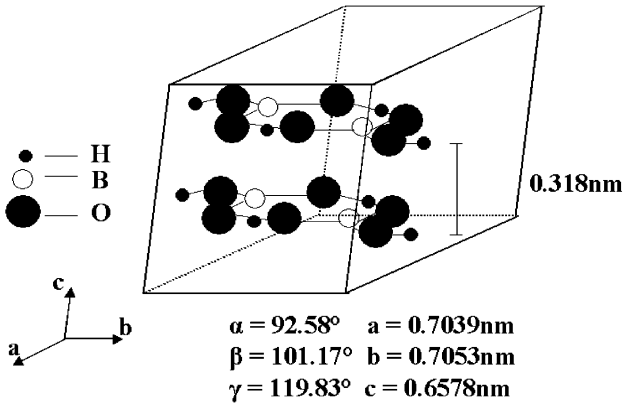

Figure 1. Schematic of the layered-triclinic structure of boric acid.

When thin coatings of boron or boron oxides,[8] or boron and boron-oxide-containing surfaces,[9] are exposed to air

* Authors to whom correspondence should be addressed. R.P.H.C. Phone: 01-847-491-3598. Fax: 01-847-491-4181. E-mail: r-chang@northwestern.edu. R.S.R. Phone: 01-847-467-6596. Fax: 01-847-491-3915. E-mail: r-ruoff@northwestern.edu.

[†] Department of Materials Science and Engineering, Northwestern University.

[‡] Department of Mechanical Engineering, Northwestern University.

(1) Lourie, O. R.; Jones, C. R.; Bartlett, B. M.; Gibbons, P. C.; Ruoff, R. S.; Buhro, W. E. *Chem. Mater.* **2000**, *12* (7), 1808.
(2) Iijima, S. *Nature* **1991**, *354*, 56.
(3) Ioan, B. *Mater. Sci. Eng.* **2001**, *B56*, 265.
(4) Remskar, M.; Skraba, Z.; Cleton, F.; Sanjines, R.; Levy, F. *Appl. Phys. Lett.* **1996**, *69* (3), 351.
(5) Nanai, L.; Thomas, G. F. *J. Mater. Res.* **1997**, *12* (1), 283.
(6) Vayssieres, L.; Beermann, N.; Lindquist, S.; Hagfeldt, A. *Chem. Mater.* **2001**, *13* (12), 4365.
(7) Erdemir, A. *Lubr. Eng.* **1991**, *47* (3), 168.
(8) Erdemir, A.; Fenske, G. R.; Erck, R. A.; Nichols, F. A.; Busch, D. E. *Lubr. Eng.* **1991**, *47* (3), 179.

10.1021/cm030261i CCC: $25.00
Published on Web 07/24/2003

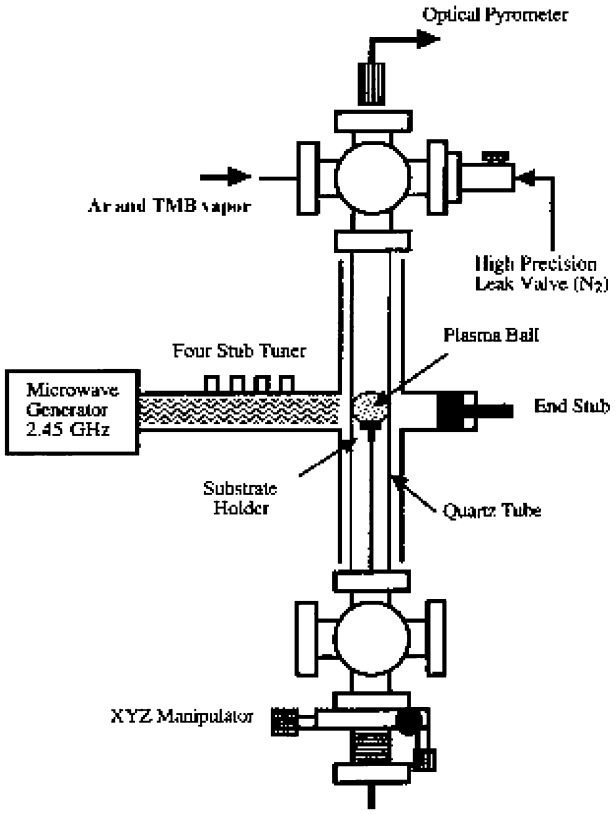

Figure 2. Schematic of the PE-CVD apparatus.

at room temperature, films of boric acid or boric acid platelets are spontaneously formed on the surface. Because of the negative standard heat of reaction, it is believed that at room temperature and when exposed to air, boron reacts with oxygen to form amorphous boron oxide on the surface, which then spontaneously reacts with the water molecules in air to form boric acid.[8] It is possible that boric acid nanostructures or microstructures could be formed by modifying the surface containing boron or boron oxide and controlling the humidity and temperature of the atmosphere.

We report the synthesis and growth properties of boric acid nano- and micro-scale structures which were spontaneously formed on the surface of films containing boron, carbon, and oxygen ("B/C/O film") after their exposure to an atmosphere with controlled relative humidity and temperature. Depending on the relative humidity, temperature, and exposure time to the humid atmosphere, these structures were either nanotubes, nanotips, nanorods, microtubes, or microtips. The dehydration of these structures in a vacuum at room temperature (23.5 ± 0.5 °C, hereafter referred to simply as 23 °C) is also discussed.

Experimental Procedure

Film Synthesis. The B/C/O thin films were synthesized by plasma-enhanced chemical vapor deposition (PE-CVD) using trimethylborate ($B(OCH_3)_3$, TMB, Aldrich, 99.5+ %) as precursor, on Si (n type, ⟨100⟩, Wafer Net Inc.) or glass (Corning 1737, Corning, Inc.) slide substrates. A schematic diagram of the PE-CVD apparatus is shown in Figure 2. The reaction chamber was evacuated to a pressure of less than 20 mTorr and then purged with Ar gas. The substrates were pretreated with Ar plasma for five minutes to clean the surface. After the pretreatment, TMB vapor was introduced into the chamber through a bubbler and Ar gas was introduced as both the carrier gas and the diluting gas. The typical flow rates of carrier Ar gas and dilute Ar gas were 0.32−2 sccm and 10−200 sccm respectively, and the pressure inside the chamber was maintained at 4−7 Torr. A 400-W microwave source was used to excite a plasma right above a graphite sample holder; the reaction time was varied from 30 s to 15 min. The temperature of the substrate was measured by an optical pyrometer. A traditional saltwater bath, which contained 23.3% (by weight) sodium chloride (NaCl) was used to provide a stable cold bath at −21.1 °C for the bubbler (At −21.1 °C, the salt began to crystallize out of solution along with the ice).[10]

Table 1. Growth Parameters of a B/C/O Thin Film

microwave power	400 W
temperature	610 °C
pressure	5−6 Torr
time	30 s
dilute Ar gas	200 sccm
carrier Ar gas	0.32 sccm
substrate	Si

XPS Experiments. A fresh thin film was made by PE-CVD using the growth conditions described in Table 1; it was then immediately transported to the XPS chamber using a small bottle filled with drierite. The XPS analyses were performed using an Omicron ESCA Probe with 1486.6 eV Al Kα radiation and a 1.5 mm beam diameter. Spectra of a rough scan from 100 to 600 eV, and fine scans of the B1s, C1s, N1s, and O1s peaks, on three random sites of the sample were recorded. All the binding energy peaks were shifted because of the insulating property of the film. To calibrate the spectra, a small amount of hexatriacontane ($CH_3(CH_2)_{34}CH_3$, 98%, Aldrich), which has a C1s peak at 284.8 eV, was added to the surface of the same sample, and the binding energy shifts of the B1s peak were calculated and adjusted to be 192.2 eV. All three sets of the spectra were adjusted by setting the B1s binding energy peaks at 192.2 eV. The relative amount of each element was obtained by calculating the area under each binding energy peak and dividing by its sensitivity factor. The sensitivity factor of carbon was set at 1.00 as a reference. The sensitivity factors of O (2.85) and N (1.77) are provided by Omicron, and were verified using poly(ethylene glycol) (Alfa Aesar) and polyacrylonitrile (Aldrich), respectively. The sensitivity factor of B was calibrated as 0.47 using B_2O_3 powder (99.98%, Alfa Aesar).

SIMS Experiments. The composition distribution in the thin film was studied by SIMS (TRIFT III ToF-SIMS, Physical Electronics) using 25 keV Ga ions as the primary ions. Negative B, C, O, and BO secondary ions were used to form the images of the composition distribution of boron, carbon, oxygen elements, and boron oxide clusters, respectively. The images were taken within areas of 50 μm × 50 μm, 10 μm × 10 μm, 5 μm × 5 μm, and 1 μm × 1 μm, on a fresh film with the same growth conditions as shown in Table 1.

(9) Vassen, R.; Stover, D. *J. Am. Ceram. Soc.* **1996**, *79* (6), 1699.

(10) Dickerson, R. E. *Molecular Thermodynamics*; W. A. Benjamin: New York, 1969.

Table 2. Growth Parameters of the Boric Acid Nanostructures and Microstructures

sample number	growth conditions (relative humidity (±3), temperature, exposure time)	incubation time (h)	morphology of the structures
8−9−02-(1−10)	20%, 23 °C, (0.083−24.62 h)	>24	nothing grows
8−11−02-(1−10)	30%, 23 °C, (0.083−48.03 h)	~0.5	t < 48 h, nanotubes; t > 48 h, microtubes
8−8−02-(1−12)	45%, 23 °C (0.17−29.83 h)	~0.2	nanorods
7−29−02-(1−6)	95%, 23 °C (0.08−48 h)	<0.08	nanorods
8−15−02-(1−12)	20%, 40 ± 1 °C (0.08−25.03 h)	~5.9	nanotips and microtips
8−13−02-(1−11)	30%, 40 ± 1 °C (0.08−24.1 h)	<0.08	t < 3.43 h, nanotubes; t > 3.43 h, microtubes and microtips
8−16−02-(1−10)	45%, 40 ± 1 °C (0.05−18.82 h)	<0.05	microtubes

XRD Experiments (To Study the Growth of Boric Acid Structures). X-ray diffraction (a Picker 2-circle diffractometer with 1.79 Å Co Kα radiation) was used to detect the growth of the boric acid structures when the fresh thin film sample was exposed to air. Fresh samples with B/C/O films on Si (100) substrates were transported immediately from the PE-CVD chamber in a drierite bottle, to the XRD sample holder sitting in air. The humidity and temperature of the atmosphere in the XRD lab were constant within 30-hour periods. A series of $\theta-2\theta$ scans from $2\theta = 15°$ to $2\theta = 40°$ were made for total times less than 30 h; thus the relative humidity and temperature in the lab were constant during XRD data acquisition.

SEM. To examine the morphology of the boric acid structures grown as a function of relative humidity, temperature, and exposure time, a series of samples were made having the same thin B/C/O film growth parameters (as shown in Table 1), but different relative humidity, temperature, and exposure time. After the PE-CVD process, the samples were immediately transported to a controlled humidity and temperature chamber. The detailed growth conditions of each sample are shown in Table 2. After a given exposure time, the samples were taken out and transported, in bottles filled with drierite, to the SEM chamber (Hitachi S-4500 FE-SEM) to examine the morphology of the nano/microstructures.

TEM and EELS. TEM samples were prepared by gently dragging the Holey (400 mesh Cu, SPI supplies) carbon grids along the surface of the samples. TEM (Hitachi H-8100 and Hitachi HF-2000), EELS (Hitachi HF-2000 with a Gatan Image Filter (GIF) system), and selected area electron diffraction (SAED, Hitachi H-8100) were used to characterize the structures present on the TEM grids.

XRD Experiments (To Study the Dehydration of the Boric Acid Structures in a Vacuum). Three separate samples were synthesized in the PE-CVD chamber at the same time, for the growth conditions shown in Table 1. They were then put in the controlled humidity and temperature chamber, which was held at 30 ± 3% relative humidity, 23 °C for 24 h. The samples were then transferred to the XRD (a Picker 2-circle diffractometer with 1.79 Å Co Kα radiation) sample chamber inside the drierite bottle. The air pressure in the X-ray chamber was kept at a constant value (which was always less than 1000 mTorr) by a mechanical pump and a separate valve. The valve controlled the flow rate to the chamber of the input air that had a constant relative humidity of 45 ± 3% at 23 °C. A series of $\theta-2\theta$ scans around the (002) peak of boric acid (~32.5°) were made until the (002) peak totally disappeared indicating all the boric acid structures were decomposed.

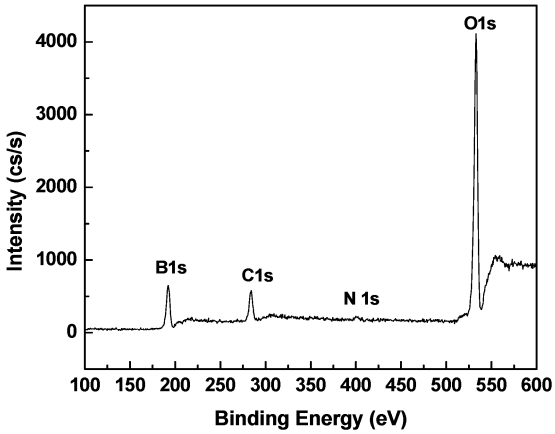

Figure 3. XPS spectrum from a fresh B/C/O film.

Table 3. Binding Energy and Relative Amount of Each Element on the Surface of the Thin Film Obtained by XPS

	site1	site2	site3
binding energy of B (eV)	192.2	192.2	192.2
binding energy of C (eV)	283.7	283.65	284.1
binding energy of O (eV)	531.9	532.9	533.05
binding energy of N (eV)	398.9	399.5	399.4
relative amounts of B (%)	43.3	39.2	41.4
relative amounts of C (%)	13.4	14.4	14.3
relative amounts of O (%)	42.8	45.7	43.2
relative amounts of N (%)	0.5	0.8	1.2

Results and Discussions

Composition, Chemical Bonding, and Element Mapping of the Thin Film. Figure 3 shows one of the typical XPS spectra from 100 to 600 eV. There are strong B1s, C1s, and O1s peaks indicating that the main composition of the film is boron, carbon, and oxygen. A very weak peak at about 399 eV shows that there is also a small amount of nitrogen in the film, which may come from residual nitrogen gas present in the PE-CVD chamber. The binding energy of each element and its relative concentration at three locations on the substrate are shown in Table 3. The average relative amounts of B, C, O, and N are 41.3, 14, 43.9, and 0.8%, respectively. The B1s binding energy at 192.2 eV and the O1s binding energy at 531.9−533.1 eV can be assigned to B_2O_3.[11−14] The C1s binding energy at 283.7−284.1 eV, which is

(11) Brainard, W. A.; Wheeler, D. R. *J. Vac. Sci. Technol.* **1978**, *15*, 1801.
(12) Burke, A. R.; Brown, C. R.; Bowling, W. C.; Glaub, J. E.; Kapsch, D.; Love, C. M.; Whitaker, R. B.; Moddeman, W. E. *Surf. Interface Anal.* **1988**, *11*, 353.
(13) Koh, M.; Nakajima, T. *Carbon* **1998**, *36* (7−8), 913.

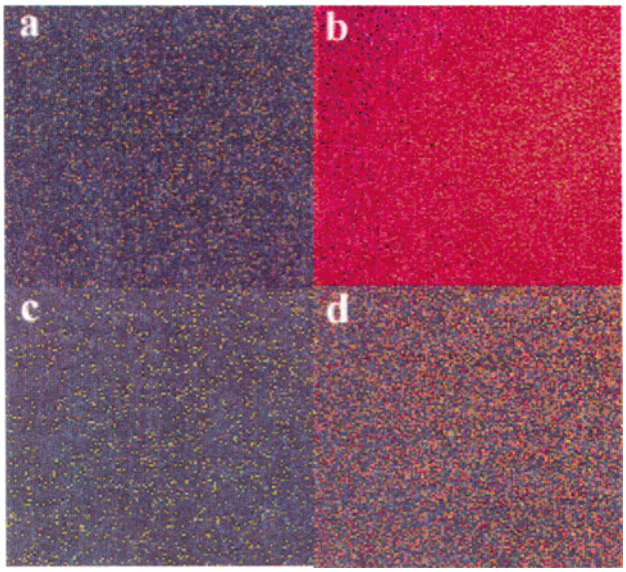

Figure 4. Composition distribution in a fresh B/C/O thin film of (a) boron, (b) oxygen, (c) carbon elements, and (d) boron oxide clusters. The images were taken by SIMS using negative B, C, O, and BO secondary ions. The size of each image is 10 μm × 10 μm.

slightly lower than the C1s peak of graphite at 284.2 eV, can be attributed to a C−C bond in boron rich sites.[13,15] The B1s binding energy and the C1s binding energy can also correspond to mixed B−C and B−O bonding (e.g., the BCO_2 group).[16] The N1s binding energy at 398.9−399.5 eV is due to the B−N bond.[17] In short, the film contains clusters of B_2O_3, BCO_2, C−C, and a small amount of B−N. These clusters are mixed randomly together and form an amorphous thin film.

All the composition distribution images taken by SIMS within areas of 50 μm × 50 μm, 10 μm × 10 μm, 5 μm × 5 μm, and 1 μm × 1 μm, are similar and suggest that the distribution of all these elements and clusters is rather homogeneous. Images taken within a 10 μm × 10 μm area are shown in Figure 4.

Growth and Morphology of the Boric Acid Nanostructures and Microstructures. Figure 5 (a) shows an XRD scan taken at 20 ± 3% relative humidity, 23 °C, and exposure time (t) 2.8 h, and Figure 5 (b) shows a scan taken at 45 ± 3% relative humidity, 23 °C, and t = 2.8 h. Figure 5 (c) and (d) show the XRD pattern of bare Si (100) substrate and H_3BO_3 powder (Aldrich, 99.999%), respectively. On Figure 5 (b), there is a peak at $2\theta = 32.5°$, which could be identified as the (002) peak of boric acid according to Figure 5 (d) and ref 18. There are no significant peaks from $2\theta = 15°$ to $2\theta = 40°$ in Figure 5 (a) (Figure 5 (a) shows only the scan data from $2\theta = 26.5°$ to $2\theta = 37°$ for simplicity). The XRD patterns in Figure 5 suggest that boric acid structures grow out of the amorphous film at 45 ± 3% relative humidity and 23 °C, whereas no crystalline

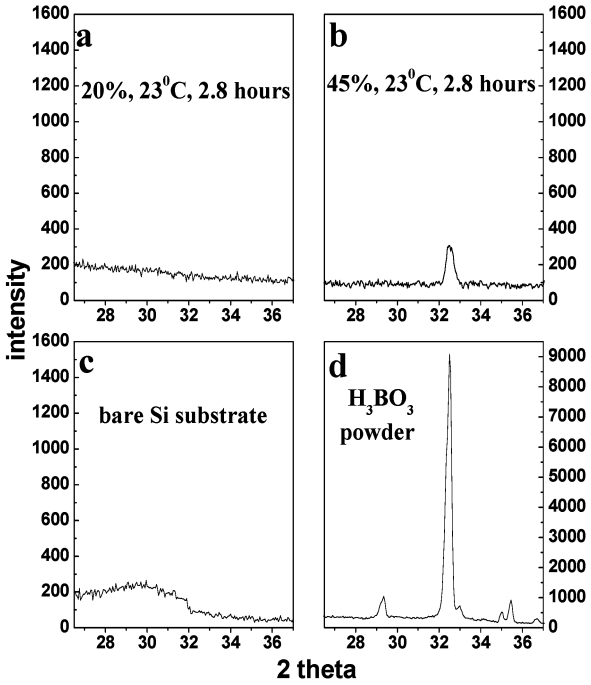

Figure 5. (a) XRD pattern of one sample at 20 ± 3% relative humidity, 23 °C, and exposure time t = 2.8 h; (b) XRD pattern of one sample at 45 ± 3% relative humidity, 23 °C, and exposure time, t = 2.8 h; (c) XRD pattern from a bare Si substrate; (d) XRD pattern from H_3BO_3 powder.

structures grow at 20 ± 3% relative humidity and 23 °C at the same exposure time of 2.8 h.

At 45 ± 3% relative humidity and 23 °C, the area of the (002) peaks of all the scans made on the same sample from 0 to 25 h were calculated and plotted versus the exposure time (t). The relative humidity and temperature were within the range of 45 ± 3% and 23 °C, from 0 to 25 h. The exposure time for each (002) peak was estimated as the time when $2\theta = 32.5°$, which is the center of the (002) peak. Since the θ-2θ scan moves evenly from $2\theta = 15°$ to $2\theta = 40°$, this time can be calculated using the start time and end time of each scan. The graph is shown in Figure 6; the inserted image in Figure 6 show the (002) peaks at t = 0.75, 1.5, 4.24, 9.08, and 23.4 h, respectively. At t = 0.75 h, the signal around 32.5° is barely above the background, which means that the amount of the crystalline boric acid structure is small. As the exposure time increases, the area of the (002) peak also increases. The rate of increase is initially high and then drops significantly above about 7 h. Because the area of an X-ray peak is proportional to the amount of the diffracting crystal planes contributing to the signal, the results indicate that the growth rate of the boric acid structure at 45 ± 3% relative humidity and 23 °C from the B/C/O thin film is high at the beginning and then drops until the equilibrium condition is achieved. The centers of the (002) peaks shift as a function of time from $2\theta = 32.53°$ at t = 2.8 h, to $2\theta = 32.63°$ at t = 23.4 h. This suggests that the d spacing (d) of the (002) plane decreases from d = 0.319 nm at t = 2.8 h to d = 0.318 nm at t = 23.4 h during the growth of boric acid nanostructures.

Figure 7 (a) and (b) show the SEM images of the nanotubes and microtubes growing out of the film, respectively. Both the nanotubes and microtubes have a cross section that is very close to a square and they

(14) Zhao, X. A.; Ong, C. W.; Ng, Y. M.; Chan, K. F.; Tsang, Y. C.; Choy, C. L.; Chan, P. W.; Kwok, R. W. M. *J. Mater. Sci. Lett.* **1997**, *16*, 1910.
(15) Shirasaki, T.; Derre, A.; Menetrier, M.; Ressaud, A.; Flandrois, S. *Carbon* **2000**, *38*, 1461.
(16) Cermignani, W.; Paulson, T. E.; Onneby, C.; Pantano, C. G. *Carbon* **1995**, *33* (4), 367.
(17) Hendrickson, D. N.; Hollander, J. M.; Jolly, W. L. *Inorg. Chem.* **1969**, *8*, 2642.
(18) Zachariasen, W. H. *Acta Crystallogr.* **1954**, *7*, 305.

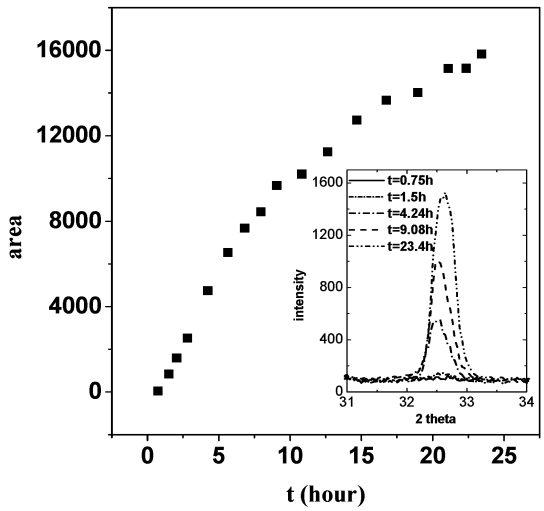

Figure 6. Plot of the area of the boric acid (002) XRD peaks from the same sample versus the exposure time (t) in air (45 ± 3% relative humidity, 23 °C). The inserted image show the boric acid (002) peaks at t = 0.75 h, 1.5 h, 4.24 h, 9.08 h and 23.4 hours, respectively.

are apparently hollow inside. The nanotubes shown in Figure 7 (a) have an average width (edge length of a square cross section) of 570 nm and an average length of 1.53 μm, for the growth conditions of 30 ± 3% humidity, 40 °C, and 0.5 h exposure time. The microtubes shown in Figure 7 (b) have an average width of 1.25 μm and an average length of 4.64 μm, and were grown at 30 ± 3%, 40 °C, and 5 h exposure time. Figure 8 (a) and (b) show the SEM images of the nanotips and microtips, respectively. The average width (measured close to the bottom) and length of the nanotips are 490 nm and 6.98 μm respectively; the growth conditions were 20 ± 3%, 40 °C, and 8.22 h. The microtips that were grown at 20 ± 3%, 40 °C, and 49.5 h have an average width of 1.37 μm and an average length of 17.5 μm. There are very tiny tips, whose diameters seem to be around 40 nm, on the tops of the nanotips and microtips. The bottoms of the nanotips and microtips are similar to those of the nanotubes and microtubes, suggesting that the nanotips and microtips are formed by capping the nanotubes and microtubes. Figure 9 shows an SEM image of the nanorods growing at 45 ± 3%, 23 °C, and 5.3 h, which have an average width of 150 nm and an average length of 880 nm. The nanotubes and nanotips observed usually have an average width larger than 300 nm, whereas the nanorods have an average width smaller than 300 nm. The different morphology of the nanostructures and the microstructures at different growth conditions is also shown in Table 2.

Figure 10 (a)−(d) show the SEM images taken on the samples, which have the same thin film growth conditions, exposed to an atmosphere of 45 ± 3% relative humidity, 23 °C, from 3 min to 29.7 h. At t = 3 min, there are no nanostructures or microstructures, all that is present is the flat film with some random defects, which suggests that there is an "incubation time" (the time needed to form enough nuclei for the growth of boric acid structures) for the growth of boric acid structures. At t = 10 min, some tiny structures and a few nanorods ∼150-nm wide and ∼750 nm long project out of the film in some areas; this provides an estimate of the incubation time of ∼10 min. The incubation times for other growth conditions are also shown in Table 2. With an exposure time of 3.24 h, many nanorods with average widths of ∼150 nm and average lengths of ∼750 nm are present. Besides the rods, a network appears on the surface (as shown in the insert image of Figure 10 (c)). The EELS spectrum of this network shows that it contains boron, carbon, and oxygen, suggesting that it may be formed by the chemical reaction between the water vapor and the whole film (note that EELS does not detect H). As the exposure time increased to 29.83 h, the nanorods grew wider and longer. The average widths and lengths of the nanorods in Figure 10 (d) are about 210 nm and 1.2 μm, respectively. The density of the nanorods in Figure 10 (d) is lower than that of the nanorods in Figure 10 (c), indicating that these nanorods may grow at the expense of the smaller ones. The inset image in Figure 10 (d) shows clearly that the nanorods tend to approach each other, which suggests that their coalescence may play an important role in the growth of larger nanorods. From Figure 10 (d), we can also see the existence of very small nanorods, which means that new nucleation events occur as the exposure time increases. Figure 10 (e)−(h) and Figure 7 (a)−(b) show the SEM images of the samples exposed to an atmosphere of 30 ± 3% relative humidity at 40 °C from 5 min to 11.8 h. At t = 5 min, lots of small clusters and a few short nanotubes appear, which suggests that the incubation time at this condition could be around 5 min. At t = 15 min, the small clusters shown in Figure 10 (e) disappear while the density and the length of the nanotubes are larger, which suggest that the nanotubes may grow by the coalescence of the small clusters. With an exposure time of 3.43 h, the nanotubes grow into microtubes with average widths of ∼1 μm and average lengths of ∼3 μm. As the exposure time increased to 11.8 h, both the microtubes and the microtips are found. All the corners of the microtubes in Figure 10(h) and also in the inserted image of Figure 7(b) project over the edges and there are also some " half capped" microtubes present. These indicate that the formation of the microtubes might be due to the higher growth rates of the corners than the edges.

Figure 11 (a)−(d) show TEM images of nanotubes, microtubes, nanotips, and nanorods, respectively. The TEM images of the nanotubes, microtubes, and nanotips show that they have hollow structures, whereas the TEM image of the nanorods indicates a solid structure. Images in Figure 11 were acquired using the Hitachi H-8100, which has a vacuum around $1 \cdot 10^{-4}$ Pa. The inset images of Figure 11 show the electron diffraction patterns of the structures, which suggest that all of the structures dehydrate into some amorphous structure in the TEM vacuum of $1 \cdot 10^{-4}$ Pa.

EELS spectra were obtained on the Hitachi HF-2000 TEM (vacuum around $2 \cdot 10^{-6}$ Pa) with a Gatan image filter (GIF) system, to explore the composition of the nano/microstructures found on the TEM grids. EELS spectra obtained from a variety of the nanostructures and microstructures are essentially identical. Figure 12 shows a typical EELS spectrum taken at the edge of a nanorod. An EELS spectrum from amorphous B_2O_3 powder (99.98%, Alfa Aesar) was also acquired for

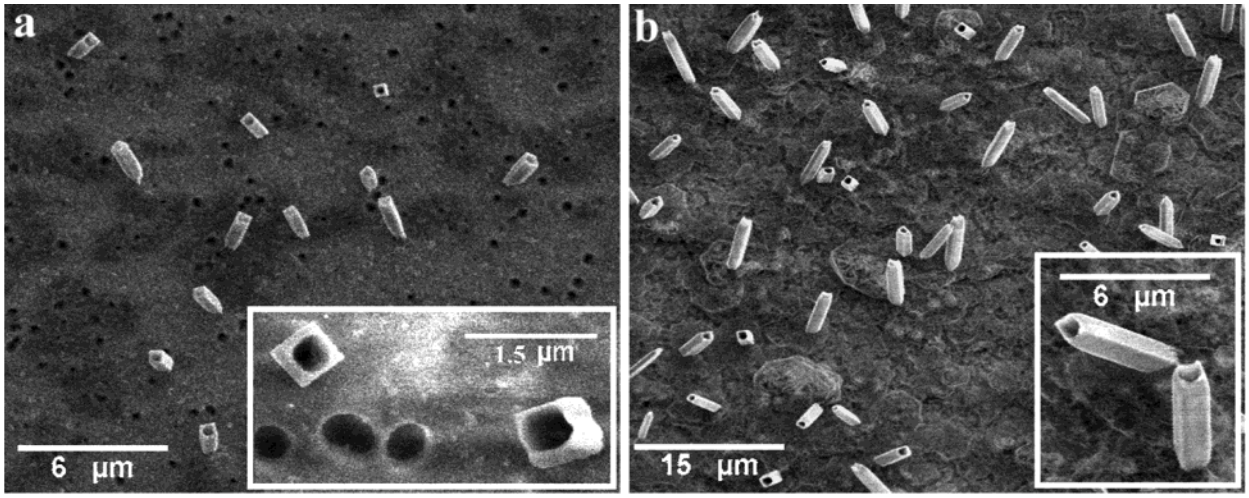

Figure 7. (a) SEM images of dehydrated (in SEM chamber, vacuum around $1 \cdot 10^{-2}$ Pa) boric acid nanotubes and (b) microtubes. Both samples had the same film growth conditions shown in Table 1, and were exposed to an atmosphere of 30 ± 3% relative humidity, 40 ± 1 °C for (a) 0.5 h and (b) 5 h.

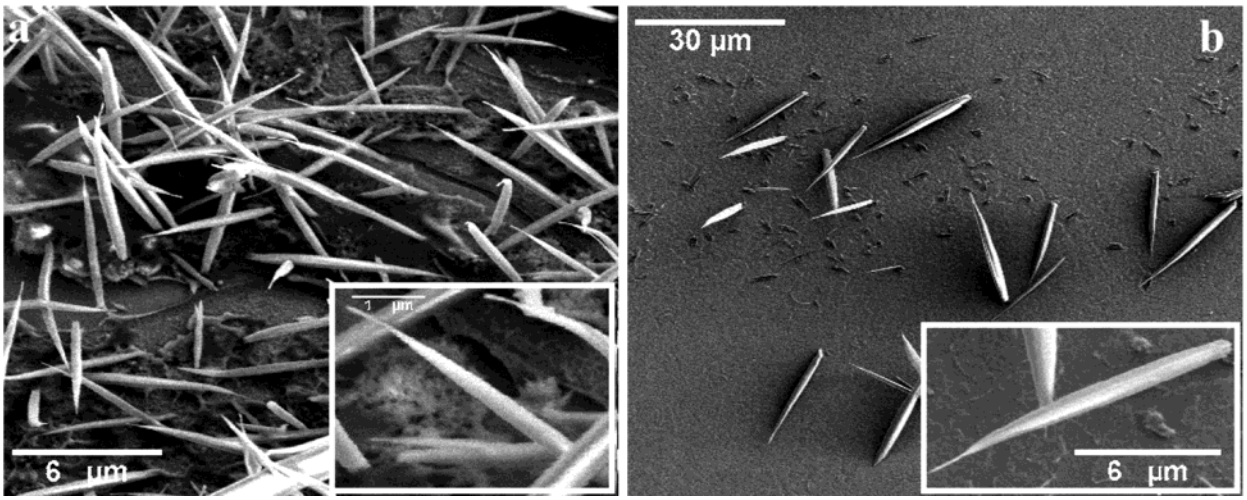

Figure 8. SEM images of dehydrated boric acid nanotips (a) and microtips (b). Both samples had the same film growth conditions shown in Table 1, and were exposed to the atmosphere of 20 ± 3% relative humidity, and 40 ± 1 °C for (a) 8.22 h and (b) 49.5 h.

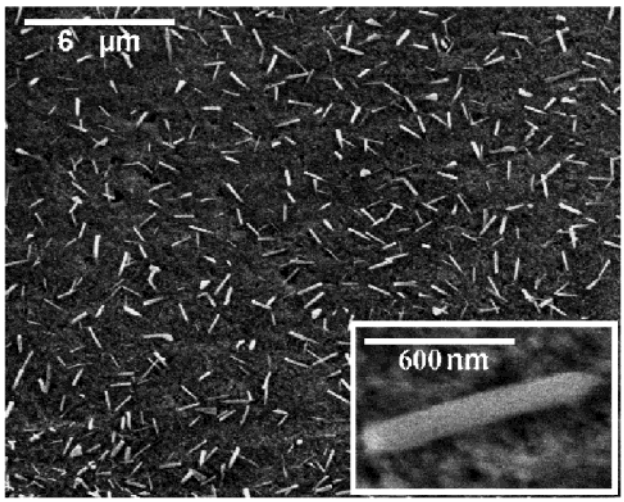

Figure 9. SEM images of dehydrated boric acid nanorods from the sample that had the same film growth conditions as shown in Table 1, and was exposed to the atmosphere of 45 ± 3% relative humidity, 23 °C for 5.3 h.

comparison. The solid line in Figure 12 is the EELS spectrum from the edge of a nanorod, and the dashed line is the EELS spectrum of the amorphous B_2O_3 powder. The close similarity of the two spectra indicates that the amorphous dehydration product of boric acid in a vacuum contains BO_3 groups and could be amorphous B_2O_3.[19,20]

Growth Process of the Boric Acid Nanostructures and Microstructures. The growth process of the boric acid structures is rather complicated. Further experiments, like in situ environmental AFM, are being carried out to fully understand the growth mechanism of the boric acid structures, and the results will be reported in a future publication. However, on the basis of the results presented above, we outline here what we observe as the growth process. When the B/C/O film is exposed to humid atmosphere, water molecules are adsorbed on the surface. The adsorbed water molecules react with the B_2O_3 clusters on the surface spontaneously and form boric acid clusters.[8] The boric acid nuclei form by coalescence of the boric acid clusters. Once the nuclei are larger than the critical nucleus size (r^*),[21]

(19) Sauer, H.; Brydson, R.; Rowley, P. N.; Engel, W.; Thomas, J. M. *Ultramicroscopy* **1993**, *49*, 198.
(20) Muramatsu, Y.; Takenaka, H.; Oyama, T.; Hayashi, T.; Grush, M. M.; Perera, R. C. C. *X-ray Spectrom.* **1999**, *28*, 503.
(21) Ohring, M. *Materials Science of Thin Film*, 2nd ed.; Academic: San Diego, CA, 2001.

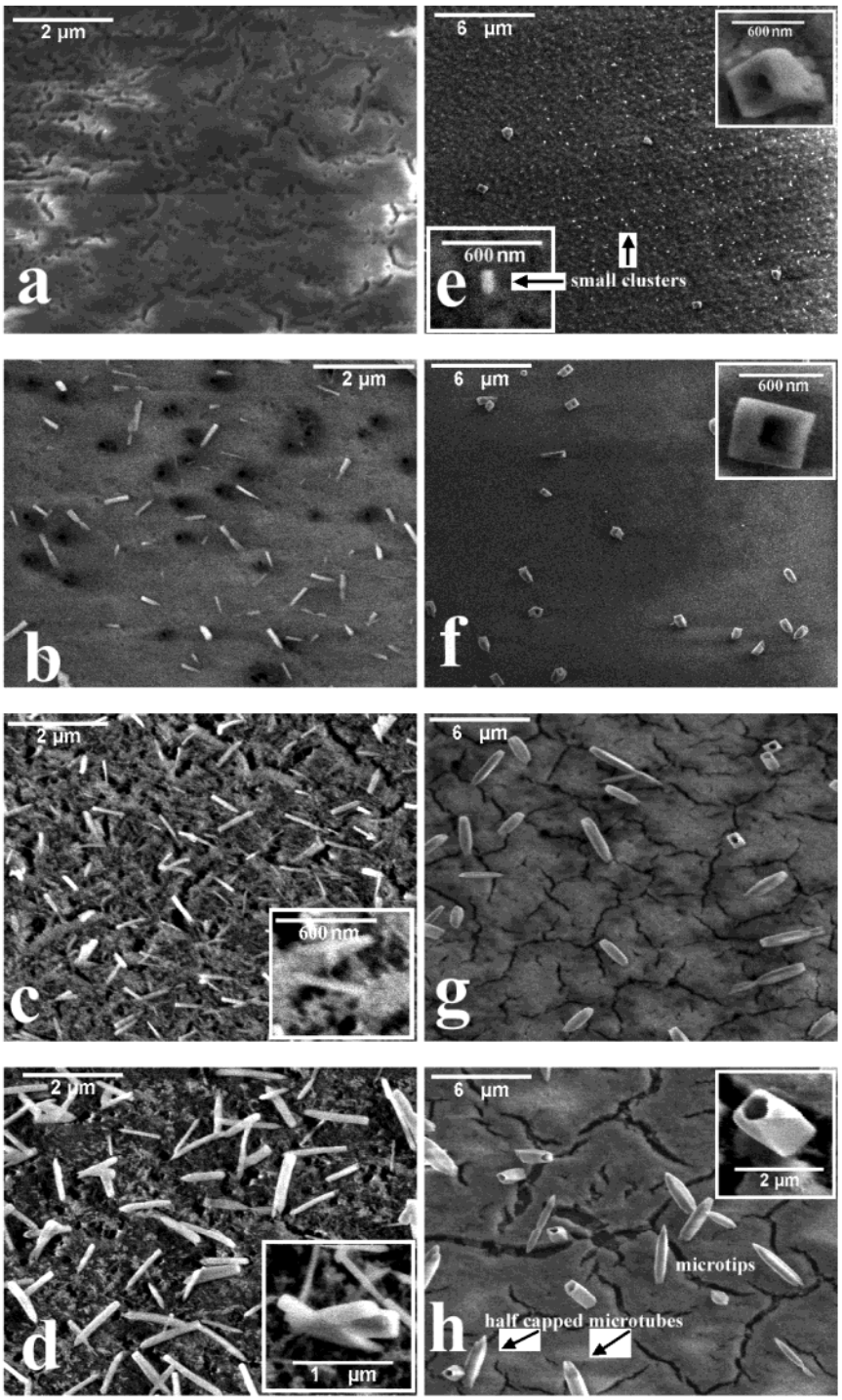

Figure 10. (a)−(d) SEM images of the samples (growth condition of B/C/O film as shown in Table 1) exposed to an atmosphere of 45 ± 3% relative humidity, 23 °C for (a) 3 min, (b) 10 min, (c) 3.24 h, and (d) 29.83 h. (e)−(h) SEM images of the samples exposed to an atmosphere of 30 ± 3% relative humidity, 40 °C for (e) 5 min (f), 15 min, (g) 3.43 h, and (h) 11.77 h.

the growth of boric acid nano/microstructures occurs. The SEM observations outlined above show that the cross section of the boric acid nano/microstructure is close to a square. We assume the morphology of the dehydrated boric acid structures in the SEM chamber, which has a vacuum around $1 \cdot 10^{-2}$ Pa, is close to the morphology of the boric acid structures. From the unit cell of boric acid shown in Figure 1, α is 92.58° (thus close to 90°), and *b* (0.705 nm) is close to *c* (0.658 nm). Thus the SEM images suggest that the ⟨100⟩ direction is the most favorable growth direction of boric acid in the experiments we have performed.

Dehydration of the Boric Acid Structures in a Vacuum. It is well-known that once heated, boric acid can dehydrate into crystallized metaboric acid (HBO_2) at 175 °C and metaboric acid can further dehydrate into crystallized boron oxide at 440 °C.[22] It is generally accepted that the following kinetic equation holds for reactions of the type

$$\mathbf{A}(s) \rightarrow \mathbf{B}(s) + \mathbf{C}(g) \quad (1)$$

$$d\alpha/dt = kf(\alpha) \quad (2)$$

where α is the fraction of reactant **A** that is decomposed,

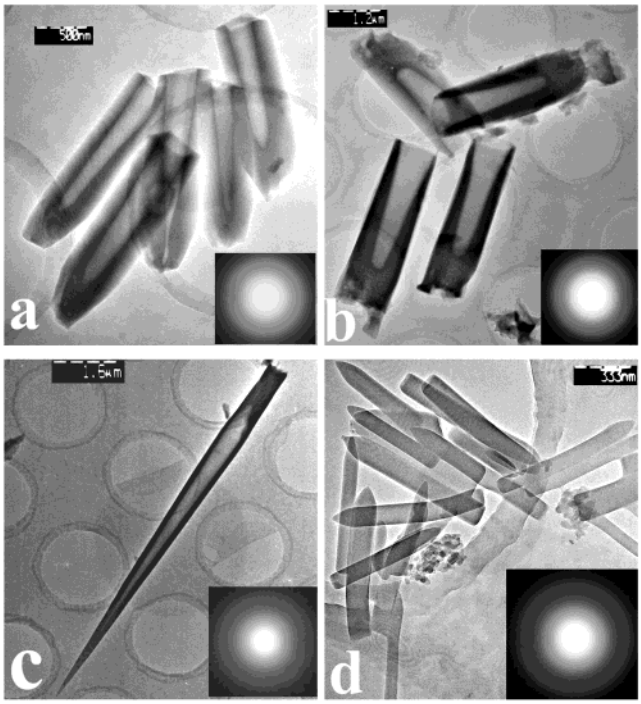

Figure 11. (a)−(d) TEM images and SAED patterns (inset in each) of the dehydrated boric acid (a) nanotubes, (b) microtubes, (c) nanotips, and (d) nanorods.

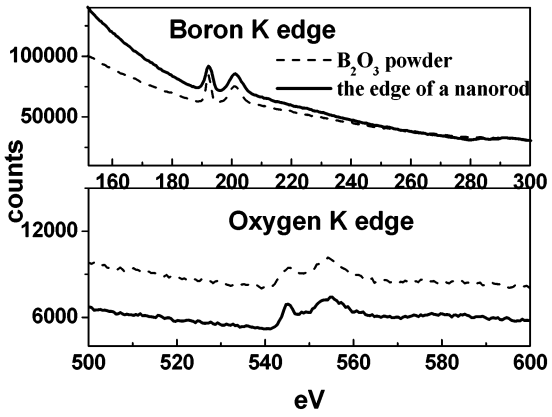

Figure 12. EELS spectrum (boron K edge upper, oxygen K edge lower) from the edge of a nanorod (solid line), and from B_2O_3 powder (dashed line).

t is the time, and k is the reaction rate constant. If we integrate eq 2, we obtain

$$F(\alpha) \equiv \int (d\alpha/f(\alpha)) = kt \qquad (3)$$

The function F(α) can be determined by fitting the experimental data of α in various theoretical functions against t.[23] Once F(α) is determined, the reaction rate constant k can be fit as the slope of F(α) vs t. Haruniko et al.[23] reported that the functional dependence of F(α) for thermal dehydration of boric acid (at 358.8 K) is $F(\alpha) = [-\ln(1 - \alpha)]^{1/2}$; we fit the slope of the plot in Figure 2 of their article, and obtain $k = 1.4 \cdot 10^{-4}$ s^{-1}.

As far as we know, the dehydration of boric acid in a vacuum has not been well studied. Scans from $2\theta = 15°$ to $2\theta = 40°$ were made on the three samples (discussed in the experimental procedure) after the (002) peaks totally disappeared. The obtained XRD patterns are similar to the one in Figure 5 (a), which means that boric acid structures dehydrate into some amorphous structure in a vacuum.

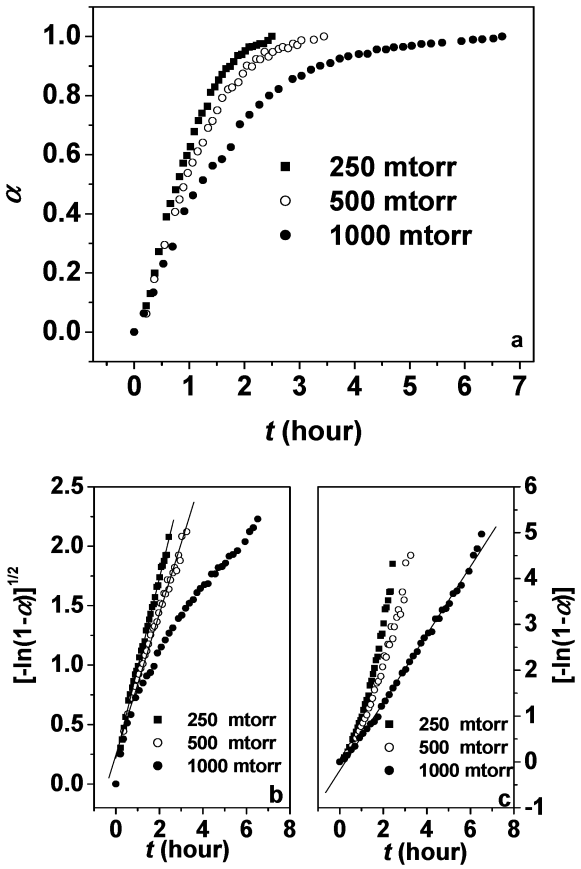

Figure 13. (a) Plot of α vs time (t), at 250, 500, and 1000 mTorr; (b) plot of $[-\ln(1 - \alpha)]^{1/2}$ vs time at 250, 500, and 1000 mTorr; (c) plot of $[-\ln(1 - \alpha)]$ vs time at 250, 500, and 1000 mTorr.

The area of the (002) peak was calculated and divided by the area of the (002) peak obtained right before pumping the XRD chamber for each sample. The value obtained should be $(1 - \alpha)$, where α is the fraction of decomposed crystalline boric acid reactant. The parameter α was plotted versus the exposure time t at different pressures and is shown in Figure 13 (a). All three curves in Figure 13 (a) have a similar shape that shows a large initial dissociation rate that continuously dropped until the reactant was completely consumed. The overall dissociation rates are different for the three samples: the higher the pressure of air, the lower the dissociation rate. Values for F(α) were obtained using the method described above for the three samples. At $P = 250$ mTorr and also for $P = 500$ mTorr, F(α) was determined as $[-\ln(1 - \alpha)]^{1/2}$, which is consistent with ref 23; at $P = 1000$ mTorr, F(α) was obtained as $[-\ln(1 - \alpha)]$. The best fit straight lines obtained by plotting $[-\ln(1 - \alpha)]^{1/2}$ versus t at 250 mTorr and also 500 mTorr, and $[-\ln(1 - \alpha)]$ versus t at 1000 mTorr, are shown in Figures 13 (b) and (c), respectively. Figure 13 also shows the plots of $[-\ln(1 - \alpha)]^{1/2}$ versus t at 1000 mTorr and $[-\ln(1 - \alpha)]$ versus t at 250 and 500 mTorr for comparison; clearly these are the incorrect functional forms. At room temperature (23 °C), 45 ± 3% relative

(22) Tanaka, H. *Thermochim. Acta* **1980**, *42*, 43.
(23) Tanaka, H. *Thermochim. Acta* **1981**, *11*, 37.

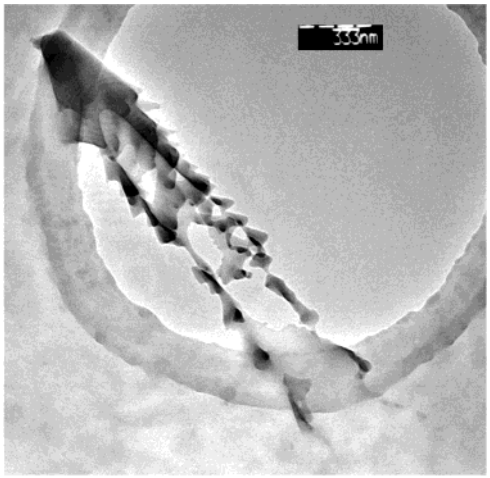

Figure 14. TEM image of a "hydrated then re-dehydrated" nanotube. The TEM grid was dragged along one sample (8−13−02−4), and put in the TEM chamber (pressure of $1 \cdot 10^{-4}$ Pa) for 2 h; one of the images taken within this 2 h is shown in Figure 11(a). The TEM grid was then taken out and exposed to air (45 ± 3% relative humidity, 23 °C) for 24 h; after that, the grid was put back in the TEM chamber again to obtain images of "hydrated then re-dehydrated" nanotubes. Figure 14 shows one of these images.

humidity (at one atmosphere pressure), the dissociation rate law of boric acid structures at 250 mTorr and 500 mTorr is $[-\ln(1-\alpha)]^{1/2} = kt$, and the constant k fit by linear regression yields $k = 2.10 \pm 0.02 \cdot 10^{-4}$ s^{-1} at 250 mTorr, and $k = 1.65 \pm 0.04 \cdot 10^{-4}$ s^{-1} at 500 mTorr; at 1000 mTorr, the dissociation rate law is $[-\ln(1-\alpha)] = kt$ and k was fit from the data to yield $k = 2.06 \pm 0.02 \cdot 10^{-4}$ s^{-1}.

When hydrated crystals dehydrate in a vacuum they typically give a phase with no clearly defined crystalline structure; the transformation is accompanied by only small changes in bulk volume and the absence of visible cracks.[24] The dehydration of boric acid in a vacuum could resemble the dehydration of many other hydrate crystals in a vacuum: an amorphous product was determined by TEM, and it had no evident cracks. In contrast, many cracks appeared in the nano/microstructures if the dehydrated structures were returned to the humid atmosphere for about 24 h and then were dehydrated again in a vacuum. The TEM image of such a "hydrated then re-dehydrated" boric acid nanotube is shown in Figure 14.

We assume the amorphous phase formed after the dehydration of boric acid crystals to be $BO_{(3+y)/2}H_y$ ($y \geq 0$); the reaction equation should be

$$H_3BO_3 \rightarrow BO_{(3+y)/2}H_y + H_2O \ (y \geq 0) \qquad (4)$$

The equilibrium partial pressure of H_2O at the phase boundary of $H_3BO_3/BO_{(3+y)/2}H_y$ can be uniquely determined when the total pressure and temperature are fixed.[25] The deviation from the equilibrium partial pressure will be the driving force for the dehydration and will thus determine the dehydration rate. The dissociation rate law is determined by the nucleation law of the phase $BO_{(3+y)/2}H_y$, the reaction rate at the phase boundary of $H_3BO_3/BO_{(3+y)/2}H_y$, and the diffusion rate of water molecules through the $BO_{(3+y)/2}H_y$ phase. The partial pressure of water at 250, 500, and 1000 mTorr (recall that the relative humidity of the inlet air to the XRD sample chamber being dynamically pumped was 45 ± 3% at 23 °C) can be calculated as 3.1, 6.2, and 12.5 mTorr, respectively; we make the assumption that the pumping rate of water is the same as the overall pumping rate of air (the saturated partial pressure of water at 23 °C is 21.08 Torr,[26] the relative humidity is 45% at 760 Torr). These numbers are much smaller than the reaction equilibrium partial pressure of water. As the partial pressure of water drops, the driving force for dissociation increases, thus the dissociation rate is larger.

The dehydration product $BO_{(3+y)/2}H_y$ formed at 250 mTorr and 500 mTorr could be the same, and could be the final dehydration product, amorphous B_2O_3. So the nucleation law of $BO_{(3+y)/2}H_y$ at 250 mTorr and 500 mTorr could be the same, which would explain the same functional form of $F(\alpha)$ at 250 mTorr and 500 mTorr. At 500 mTorr, both the reaction rate at the $H_3BO_3/BO_{(3+y)/2}H_y$ interface and the diffusion rate of water molecules through the $BO_{(3+y)/2}H_y$ phase are lower than those at 250 mTorr, so the dissociation rate constant k is lower than that at 250 mTorr. At 1000 mTorr, the value of y in the dehydration product could be larger than that at 250 and 500 mTorr, which means the boric acid structures partially dehydrate into some amorphous structure containing boron, oxygen, and hydrogen. This hypothesis explains why the nucleation of $BO_{(3+y)/2}H_y$ at 1000 mTorr probably differs from the one at 250 and 500 mTorr, which offers an explanation for the different functional form of $F(\alpha)$.

Conclusion

Thin films containing mainly boron, carbon, and oxygen were synthesized by PE-CVD using trimethylborate as a precursor. Once exposed to humid air, boric acid nanostructures and microstructures grew on the thin B/C/O film. Depending on the relative humidity, air temperature, and exposure time, these structures were either nanotubes, nanotips, nanorods, microtubes, or microtips. The nanostructures and microstructures have a crystalline boric acid structure at one atmosphere pressure and dehydrate to yield similarly shaped amorphous structures in a vacuum. Their dissociation in a vacuum obeys different dissociation rate laws at different pressures.

The growth of boric acid structures involves: (a) the adsorption of water, (b) the nucleation of boric acid clusters (c), and the preferred growth of the nuclei along the ⟨100⟩ direction.

To our knowledge, this is the first report of the formation of boric acid nanometer- or micrometer-sized tubes, tips, and rods. These novel structures could have potential applications in submicron-scale devices and sensors. Their unique properties, such as self-lubrication[7] and dehydration in a vacuum may have promising applications in tribology and other areas.

(24) Garner, W. E. *Chemistry of the Solid State*; Butterworth Scientific Publications: London, 1955.

(25) Schmalzried, H. *Solid State Reactions*, 2nd ed.; Verlag Chemie: Deerfield Beach, FL, 1981.

(26) *Handbook of Chemistry and Physics*, 73rd ed.; CRC Press: Boca Raton, FL, 1992−93.

Acknowledgment. This work has been supported by the Semiconductor Research Corporation (SRC) and B NIRT NSF grant (29212S/WU-HT-02-33/NSF-EEC-0210120). We appreciate helpful discussions with Dr. Nianqiang Wu (on XPS and SIMS experiments), Dr. Kai Zhang, Xiang Liu (on XRD experiments), and Dr. D. Bruce Buchholz (on proposed growth mechanism). We acknowledge the use of MRSEC facilities: the J.B. Cohen XRD Facilities, EPIC (Electron Probe Instrumentation Center), and the Keck Interdisciplinary Surface Science Center at Northwestern University.

CM030261I